RANDOM MAGNETIC ANISOTROPY EFFECTS IN GLASSES BASED ON $Gd_{65}Co_{35}$

by

FAUZIAH OTHMAN

B.S., Kansas State University, 1983

A MASTER'S THESIS

submitted in partial fulfillment of the

requirements for the degree

MASTER OF SCIENCE

Department of Physics

KANSAS STATE UNIVERSITY
Manhattan, Kansas

1985

Approved by:

Michael J. O'Shea
Major Professor

ACKNOWLEDGEMENTS

I thank God Almighty for the strength to carry this work through.

I dedicate this work to my late father and my mother for their love and encouragement.

I'm deeply indebted to my Major Professor, Dr. M.J. O'Shea for his guidance and concern throughout the course of this work. His knowledge and untiring assistance have been of great benefit and are genuinely appreciated.

I would like to acknowledge Malaysian Ministry of Education for the financial support that has made my study here possible.

I would like to express my gratitude to Dr. D.J. Sellmyer, Dr. G. Hadjipanayis and Dr. D. Dragsdorf for the extensive use of the Splat Cooling Apparatus, DSC facilities and X-ray facilities respectively.

To the faculty and staff of the Physics Department, and my fellow graduate students, I thank them for their help and friendliness.

TABLE OF CONTENTS

Page

LIST OF FIGURES

Page

Page

LIST OF TABLES

CHAPTER 1

INTRODUCTION

The magnetic properties of metallic glasses have been a subject of interest even before ferromagnetism was first observed in them two decades ago. Gubanov in 1960, found long-range ferromagnetic exist in amorphous systems [1]. About a decade ago, Rhyne et al. [2] discovered several unique features in the properties of glasses containing anisotropic rare-earth elements. More recently Harris, Plischke and Zuckermann (HPZ) presented a theory in which site-to-site variations in the anisotropy direction were considered to explain a number of the properties of these glasses [3]. The HPZ Hamiltonian incorporating a local random anisotropy (LRA) may be written as:

$$H = -I\sum_{ij}(\vec{S}_i \cdot \vec{S}_j) - D\sum_{i}(\hat{n}_i \cdot \vec{J}_i)^2 \qquad (1)$$

The first term is the exchange and the second term represents the LRA; $\hat{n}_i$ is a random unit vector describing the local direction of magnetic anisotropy. Rare-earth metallic glasses show a wide range of magnetic behavior ranging from ferromagnetism to a spin-glass-like state, due to the presence of LRA. Recently, the theoretical situation for the LRA has seen several new predictions and we shall refer to these in the following chapter. In addition, the character of the 'transition' in the LRA case is obscure but there are indications that it may be related to the paramagnetic-spin-glass transition.

It is the purpose of this thesis to present further studies on rare-earth-rich glasses and to compare experimental results with recent

theoretical predictions. We focus on a variety of rare-earth-rich glasses of the nominal form $Gd_xCo_{35}RE_{65-x}$ where RE denotes Ce, Pr, Nd, Tb, Dy, Er and $35 \preceq x \preceq 65$. The terms amorphous rare-earth alloys and rare-earth glasses are used interchangeably in the text. LRA is introduced in a controlled manner by alloying with anisotropic RE's. Samples were prepared by the splat cooling technique and X-ray analyzed to ensure that the structure is amorphous. In the following chapters we shall

(a) briefly review recent theoretical advances in the LRA problem and some previous work.

(b) discuss the effect of the magnitude of LRA on the character of the phase transition.

(c) report on 're-entrant' transitions (Ferromagnetic to Speromagnetic) observed in anisotropic rare-earth-rich glasses.

(d) motivate using the idea that some type of anisotropy is required to produce spin-glass behavior.

(e) try out some scaling analyses.

(f) observe the magnetic hardness of the LRA glasses.

Rare-earth glasses are generally of great interest not only from a fundamental point of view as discussed above but also because of their potential as magnetic information storage media, and because of the high coercivity present in some of these materials.

CHAPTER 2

THEORETICAL DEVELOPMENTS

2.1 The Model Hamiltonian

To provide a framework for the discussion of magnetic properties of rare-earth glasses, we consider the model Hamiltonian

$$H = -\sum_{ij} (I + \Delta I_{ij})\, \vec{S}_i \cdot \vec{S}_j \; - D\sum_i (\hat{n}_i \cdot \vec{J}_i)^2 \qquad (2)$$

The first term represents the exchange in the system. I is an average ferromagnetic exchange, ΔI_{ij} represents the exchange fluctuations, $<ij>$ denotes a pair of spin sites and $\vec{S}_i$ is an m-component spin vector located at the lattice site i. If $<I_{ij}> \geq I$ then there will be significant antiferromagnetic interactions in the system. The second term represents a single-ion uniaxial anisotropy. $\hat{n}_i$ is a unit vector describing the anisotropy direction (easy direction) which varies at random in direction from site-to-site and D represents the strength of anisotropy. For the ordered crystalline material, this anisotropy has a well defined direction along one of the coordinate axes (magnetocrystalline anisotropy). The randomness of the anisotropy field is an important characteristic of the amorphous state (each spin is subjected to a local anisotropy field of random orientation - LRA). If D is taken to be zero, Equation (2) becomes the Hamiltonian on which much of the spin-glass problem is based. If ΔI_{ij} is taken to be zero, Equation (2) becomes the Harris-Plischke-Zuckermann (HPZ) Hamiltonian on which much of the theory of the LRA problem is based. It is important to realize, however that rare-earth glasses are alloys so that, in general,

all the components of Equation (2) will be required to describe in detail a real material.

Figure 2.1 is a schematic phase diagram of possible magnetic states in the presence of LRA and exchange fluctuations [4] and $t \equiv K_B T/I$, $d \equiv D/I$ and $\delta \equiv \langle \Delta I \rangle / I$. In the d = 0 plane, one has the possibility for ferromagnetic (FM), spin-glass (SG) and mixed (M) phases. M refers to cases where there may be freezing of transverse or longitudinal components of the spins. In the $\delta = 0$ plane, the speromagnetic (SM) phase refers to a frozen, random magnetic structure with no long-range order much like a spin-glass state; the difference is that the former is produced by the presence of an LRA while the latter is produced by the presence of antiferromagnetic (AFM) interactions. The correlated speromagnetic state (CSM) in Figure 2.1 is different from a multidomain ferromagnet in that magnetization rotates smoothly through the sample and there are no sharp domain walls [5]. The existence of CSM is predicted in amorphous two-subnetwork magnetic glasses by Serota and Chudnovsky [5]. For example, in an amorphous ferromagnet, the addition of LRA should transform this state into a CSM state in which locally the magnetizations of the subnetworks are antiparallel but they rotate smoothly throughout the sample. The existence of the CSM and mixed states is somewhat questionable in real systems and we will not be concerned with these states in our systems. It should always be borne in mind that one probably cannot have a material relevant to either the t-d or t- δ planes. Thus, considerable caution is needed when comparing data

to theories for either case. Figure 2.2 illustrates the varieties of the magnetic order that are thought to exist in one- and two-moment subnetwork glasses. In particular the speromagnetic state is similar to that of a spin-glass.

2.2 Local Random Anisotropy (LRA)

In amorphous rare-earth-based alloys magnetic exchange can be viewed as consisting of three basic mechanisms in analogy to the crystalline laves phase compounds:

(i) a direct exchange between neighbouring transition metal ions I_{TM-TM}

(ii) a competing antiferromagnetic or ferromagnetic exchange between the rare-earth and the transition metal ions I_{TM-RE}

(iii) a weaker indirect coupling between the rare-earth ions I_{RE-RE}

In non-S-state rare-earth based alloys there is present an additional strong perturbation from the local anisotropy interaction.

In an amorphous material anisotropy can originate from the spin-orbit coupling. It occurs in materials containing non-S-state ions, mostly from the direct electrostatic interaction between the non-spherical electronic charge distribution and random electric field gradients. These electric field gradients are the amorphous analog to the crystalline field. The positional disorder of the rare-earth ions generates random electric field gradients. The anisotropic (non-zero orbital angular momentum) rare-earth ions interact with these fields to produce a preferred orientation of the magnetic ion: a single-ion anisotropy. The anisotropy effects differ from conventional

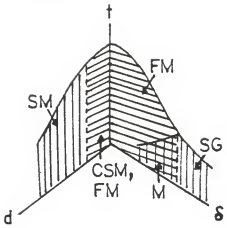

Fig. 2.1 Schematic phase diagram of possible magnetic states in the presence of LRA and exchange fluctuations (see text).

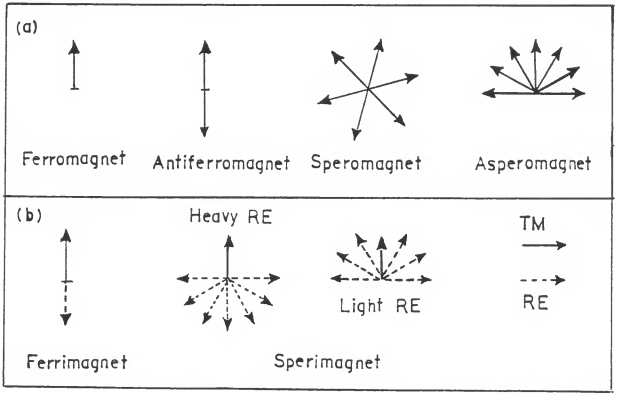

Fig. 2.2 Possible (a) one-subnetwork and (b) two-subnetwork magnetic structures.

magnetocrystalline anisotropy in the sense that they do not give rise to any bulk easy axis of magnetization. Each ionic spin is subjected to a local anisotropy field of random orientation. Harris, Plischke and Zuckermann (HPZ) have developed a model particularly appropriate to such rare-earth alloys in which each ionic spin is subjected to a local anisotropy field of random orientation [3]. The HPZ Hamiltonian is written as Equation (1) given in Chapter 1. Equation (1) is a simplified version of Equation (2) with I assumed to be constant, so exchange fluctuations are assumed to be negligible.

If D and I are assumed to be positive, then qualitatively there will be a competition between the ferromagnetic coupling term and the 'spin scattering' effect of the assumed uniaxial anisotropy. The particular point of interest is to vary the ratio of D/I from close to zero to a very large value. In the case D = 0 the Hamiltonian represents a Heisenberg system in which a ferromagnetic state is expected at sufficiently low temperatures. For small D/I, arguments similar to those of Imry and Ma [6] give a correlation length ξ which varies as $(D/I)^{-2}$ for three dimensions [7]. At some small value of D, ξ will become less than the sample diameter and it will be energetically favorable for domain formation to occur. For large D/I the spins will be pinned along their local easy axis at sufficiently low temperatures and a frozen-in speromagnetic state will result. Aharony and Pytte [8] have determined the magnetic equation of state for small H/M and small D/I. The authors [9] concluded that the susceptibility was limited for $T < T_c$ to

$$\chi^{max} \sim (I/D)^4 \qquad (3)$$

This result implies a finite susceptibility for finite D and infinite susceptibility only when D = 0. This result has been verified by several other calculations [5, 10]. In the intermediate regime where $D/I \approx 1$ the correct description of the magnetic structure is not clear.

Recently, Dotsenko and Feigelman [10] studied the three dimensional planar magnet (XY model) with random anisotropy fields for various orders of anisotropy, n = 1, 2, 3, ... n = 1 and n = 2 correspond to the random field and random anisotropy cases respectively. These authors calculated the zero-field susceptibility and find for the LRA case a cusp-like behavior in $\chi(T)$. However, there is a region ΔT near T_c which is outside the range of validity of the calculation. As T approaches T_c, the authors find behavior that is 'so far rather obscure', but no evidence for an infinite susceptibility phase was found in agreement with the calculations of Aharony and Pytte.

2.3 Exchange Fluctuations (RKKY Interaction)

Indirect exchange is important in most metallic systems where direct exchange is not present. Examples are:

(i) In rare-earths where the magnetic 4f shells are well localized and so do not overlap.

(ii) In metallic systems containing small amounts of transition metals (d-shells do not overlap).

The RKKY interaction named after its principal investigators, Ruderman, Kittel, Kasuya and Yosida [11] is unique because J oscillates from positive to negative (so the coupling between the magnetic moments of two

impurity spins can be either FM or AFM) as the separation between the ions change. It's form is shown in Figure 2.3 where $J(r) \sim \cos 2K_F r/(K_F r)^3$ as r goes to infinity where K_F is the Fermi wave-vector. This interaction is restricted to materials containing itinerant electrons, which are the intermediaries in the coupling. A magnetic ion induces an oscillatory spin polarization on the conduction electrons in its neighborhood. This polarization is oscillatory because the conduction electrons try to screen out the magnetic moment on the ion by the means of their spins but their wave functions have a limited range of wavelengths. The strength of this screening polarization decreases with increasing distance from the ion, but its effect has a relatively long range. This modulated spin polarization in the itinerant electrons is felt by the moments of other magnetic ions within range, leading to an oscillatory, indirect coupling.

In a disordered metallic system, where the separation between magnetic ions is random, the magnetic interactions are also randomly distributed. The possible conflicts in the system on a microscopic scale as moments try to respond to antagonistic constraints (Figure 2.4) bring about frustration. A frustrated system is one which is not able to achieve a state that satisfies entirely its microscopic constraints and possesses a multiplicity of equally unsatisfied states. A frustrated system, therefore, has no unique microscopic arrangement for its ground state; there is an essentially infinite number of equivalent states that can be adopted. This gives rise to the term spin-glass where the atomic spins are without order or regular structure. Spin-glass systems show

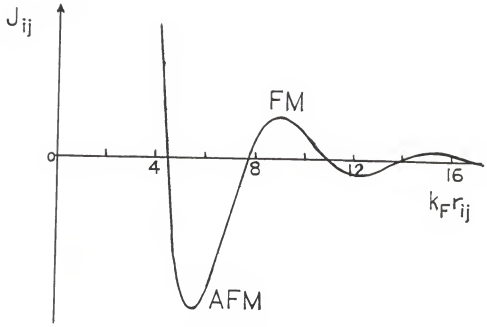

Fig. 2.3 The RKKY interaction J (r) between two magnetic impurities as a function of their separation.

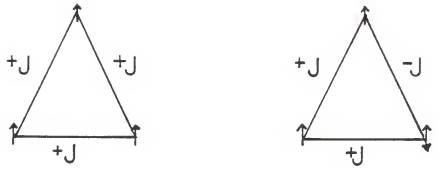

Fig. 2.4 A triangular lattice of Ising spins (the spin can be either up or down) illustrates the concept of frustration.

metastability, with hysteresis effects and time-dependent relaxation towards an equlibrium state.

If D is taken to be zero, Equation (2) becomes the Hamiltonian on which the spin-glass problem is based.

$$H = - \sum_{ij} (I + \Delta I_{ij}) \vec{S}_i \cdot \vec{S}_j \qquad (4)$$

This Hamiltonian allows for fluctuations of exchange through the ΔI_{ij} term.

2.4 Similarities between the LRA and SG States

Topological disorder in amorphous alloys leads to distributions of random fields at the atomic scale. Two cases which we have considered in the previous two sections are: 'amorphous spin-glasses' in which a random exchange field results from a wide distribution of positive and negative exchange interactions with an average value I, and 'random anisotropy-dominated magnets' with essentially positive exchange interactions at the atomic scale and a distribution of local anisotropy directions, leading to a random anisotropy field.

An important question is whether the spin-glass and speromagnetic transitions are continuous phase transitions, akin to that in many amorphous ferromagnets. We are particularly concerned with the nature of the phase transition they undergo at a temperature T_c between the paramagnetic and low temperature phases. A high level of theoretical interest has been sustained in the LRA problem. Aharony and Pytte [8] pointed that the LRA systems should have qualitatively different characteristics from those of ferromagnets. Pelcovits, Pytte and Rudnick [12] showed that if the number of spin components $m \geq 2$, there is no

long-range ferromagnetic order in the LRA model for $d \leq 4$ implying that the lower critical dimensionality is 4. Several studies [13] (of which none of the arguments is absolute) suggests $d \leq 4$ for Ising spins.

Chen and Lubensky [14] showed an important connection between the LRA and SG problems, viz., for sufficiently large D the effective energy density has the same form as that of the random bond Ising SG model using Ising symmetry. The spin-glass phase with random exchange interactions is characterized by a vanishing average moment $[\langle \vec{S} \rangle]_{av} = 0$ but a non-vanishing moment squared, $[\langle \vec{S} \rangle \cdot \langle \vec{S} \rangle]_{av}$. Here $\langle \vec{S} \rangle$ refers to the thermodynamic average and $[\ ]_{av}$ refers to an average over the ensemble of random exchanges. In the HPZ model, each magnetic ion is subjected to a local anisotropy field of random orientation. It is clear how this model might produce a spin-glass-like state. For sufficiently strong anisotropy, the spins follow the local anisotropy axis. Since this axis has a random orientation, $[\langle \vec{S}(\vec{x}) \rangle]_{av} = 0$. At low enough temperatures, however, $[\langle \vec{S}(\vec{x}) \rangle \cdot \langle \vec{S}(\vec{x}) \rangle]_{av}$ is non-zero. Thus, the HPZ model can have an Ising spin-glass transition if D is sufficiently large. Aharony failed to find a stable ferromagnetic fixed point for this system in $4 - \epsilon$ dimensions [15]. It is possible that the flow away from the ferromagnetic fixed points is to the above spin-glass fixed point.

Both types of random magnets (amorphous spin-glass and anisotropy-dominated random magnets) show a cusp in the field-cooled susceptibility at T_c with susceptibility itself much less than the ferromagnetic limit. An example is shown in Figure 2.5 [16, 17]. SM and

Fig. 2.5 Similarities between SG and SM states.

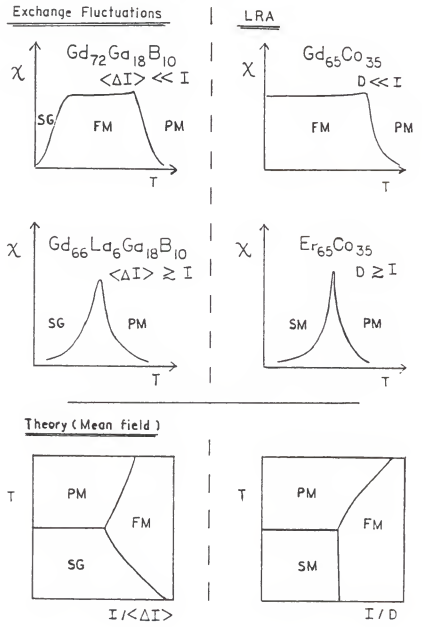

SG states are characterized by the same order parameters in the mean field theory.

There are many similarities between the two problems. In summary

(i) Both systems were thought to have a lower critical dimensionality of 4 (no long-range order may exist below this dimensionality).

(ii) The mean field free energy has the same form for both systems (if D is sufficiently large).

(iii) The magnetic susceptibility of both systems shows a cusp at T_c

(iv) SM and SG states are characterized by the same order parameters in mean field theory.

2.5 Scaling Theory of a SG Transition

To decide whether the spin freezing at T_c is a thermodynamic phase transition, it is necessary to measure the critical behavior. Assuming the PM-SG transition is a true phase transition (not proven) we will try to describe the susceptibility measurement. We can define the non-linear magnetization (see Figure 2.6) as

$$M_S = \chi_o(T)H - M \tag{5}$$

With the above assumptions Chalupa [18] has shown that the magnetic equation of state for small ϵ and H may be written

$$\frac{M_S}{\epsilon^{(\gamma+3\beta)/2}} = g\left[\frac{H}{\epsilon^{(\gamma+\beta)/2}}\right] \tag{6}$$

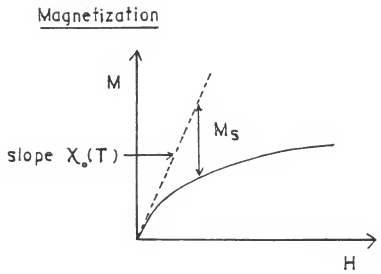

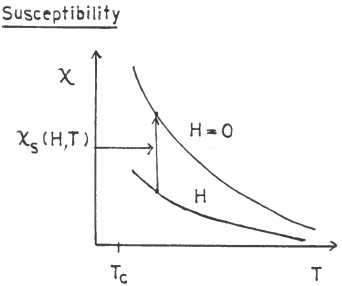

Fig. 2.6 Non-linear magnetization and non-linear susceptibility.

where $\epsilon = \left(\frac{T_o - T_c}{T_c}\right)$ and $\gamma + \beta = \beta\delta$. β and δ are two adjustable parameters. From the scaling expressions of M_s above one obtains the following functions for the susceptibility by differentiation

$$\chi_s = \frac{dM_s}{dH} = \chi_o(T) - \chi(T,H) \tag{7}$$

and $$\frac{\chi_s}{\epsilon^{\beta}} = f\left[\frac{H}{\epsilon^{(\gamma+\beta)/2}}\right] \tag{8}$$

χ_o is the linear susceptibility for the H = 0 and $\chi(T,H)$ is the non-linear susceptibility (see Figure 2.6) in finite fields.

2.6 Systems to Be Studied and Previous Works

In this thesis we shall study the magnetic properties in rare-earth-rich glasses of the nominal form $Gd_xCo_{35}RE_{65-x}$ where Re = Ce, Pr, Nd, Tb, Dy, Er and $35 \preceq x \preceq 65$. Rare-earth elements are convenient for magnetization studies since their moments are highly localized and well defined. Normal rare-earth metals exhibit a rather clear distinction between 4f electrons responsible for the existence of local moments and itinerant electrons responsible for the interactions between moments. The rare-earths discussed here normally adopt a trivalent 4f configuration in alloys except Ce which is sometimes quadrivalent. The RE elements and composition ranges were selected to provide a variation in the parameter D/I, the ratio of the single-ion anisotropy to exchange constant. The presence of the 'glass former' atom (Co) is also of critical importance. A Co concentration of 35% was chosen because of the relative ease of making amorphous $RE_{65}Co_{35}$ samples with the splat-cooling technique (section 3.1). It has been noted that for RE-Co alloys

the Co ion retains its moment even at Co concentration as low as 35% [17, 19], where it has a moment of less than 1 μ_B compared to 7.9μ_B for Gd. However, it is necessary first to understand the exchange interaction before the role of random anisotropy can be separately identified. For this reason we start with the alloys with RE = Gd. Gd^{3+} ($4f^7$, J = 7/2) is an S-state ion, and single-ion anisotropy is expected to be negligible.

The amorphous alloys of Gd offer the least complex magnetic behavior of the rare-earth-rich glasses due to the absence of LRA interactions in this S-state (orbital quantum number L = 0) ion. It is clear that observation of the ferromagnetic or CSM state is most likely to occur in Gd rich glasses. This follows since to first order there is no orbital angular momentum and thus no single-ion anisotropy. However, there could be a weak anisotropy due to a small admixture of higher L-states into the ground states. Calculations by Wybourne [20] show that the Gd^{3+} ground state is split as a result of the intermediate coupling of other L, S states into the ground state. This mixing in of states with orbital angular momentum will give rise to a single-ion anisotropy as in the HPZ equation.

Preliminary accounts on work done on $Gd_{65}Co_{35}$ [17, 21] have shown that the sample is magnetically ordered below a temperature T_c. A simple localized model was suggested for this alloy and their inverse susceptibility shows a Curie-Weiss behavior. The Co spins are coupled ferrimagnetically to Gd [22, 23]. The existence of ferrimagnetic coupling is consistent with the negative exchange coupling seen between

Gd and Co moments in the Gd-Co-Mo alloys [24]. For temperatures above T_c, the data [17] were fitted to a Curie-Weiss law. They found the Curie-Weiss temperature $\theta = 187 \pm 3$ K.

Studies have been done on $Gd_{72}Ga_{18}B_{10}$, $Tb_{72}Ga_{18}B_{10}$, $Nd_{64}Ga_{16}B_{20}$ [25, 26] and on $Gd_{65}Co_{35}$, $Er_{65}Co_{35}$, $Nd_{64}Co_{36}$ [17]. They show that for the Gd glasses an extremely large possibly infinite susceptibility is present below T_c, whereas the Tb, Nd and Er glasses, all of which have large anisotropy exhibit transitions to a speromagnetic state and do not show an infinite susceptibility phase. Studies have also been done on $RE_{69}Co_{31}$ where RE = Gd, Nd, Tb, Dy, Er [27] and on $RE_{65}TM_{35}$ where RE = Er, Nd, Gd [17]. Most of the alloys in which the RE component has an orbital momentum were found to exhibit large intrinsic coercive forces at low temperatures. This magnetic hardness is in agreement with the presence of LRA in the non-S-state ions.

CHAPTER 3

SAMPLE PREPARATION AND CHARACTERIZATION

3.1 Sample Preparation

For this thesis, alloys of nominal composition $Gd_xCo_{35}RE_{65-x}$ where RE denotes Ce, Dy, Er, Nd, Pr, Tb and x = 65, 61, 55, 45, 35 were made with elemental constituents of at least 99.9% purity (Research Chemicals, Phoenix, Arizona).

A polycrystalline 'button' (1 g) of the appropriate stoichiometry was prepared. The materials were weighed and stoichiometrics were known to about 0.01 atomic % before melting. Prior to melting, the materials were cleaned with acetone to rinse off any dielectric oil which contaminated the materials. The elements in their proper proportions were melted under a purified argon atmosphere in a water cooled copper hearth by an arc furnace. A Centorr Series 5 Single Arc Melting furnace was used. This consists of a 3" diameter cylindrical pyrex observation tube with a water cooled copper top and bottom. A copper welding rod which acts as the cathode is fitted with a bakelite handle through a fixture at the top. The materials were placed in a removable hearth that fits the copper base (anode). An arc was produced by moving the tungsten electrode close to the copper anode. During the melt prepurified argon gas flows continuously. The 'button' was turned to ensure proper mixing and arc melted again. Each melt proceeded by maintaining an arc for about 8 second at $\sim$ 55 amps. For the alloys discussed here the final buttons have less than 0.1 mass % loss.

The amorphous samples were prepared by the splat cooling technique in an atmosphere of purified argon gas [28]. Figure 3.1 shows a schematic of the 'splat cooling technique.' In this method a small portion (0.25 g - 0.3 g) of the original button was remelted and then squeezed between two cool surfaces which have rapidly come together. A basic requirement for producing amorphous metallic materials from the melt is very rapid cooling of the alloy at rates of 10^6 degrees per second or higher. Otherwise, microcrystalline or macrocrystalline material will be produced. The resulting foils were disks 2-3 cm in diameter and about 50 μm thick. Structure of specimens from the foils was studied using a transmission electron microscope. The diffraction patterns showed two diffused halos indicating that the samples were amorphous. It has been noted that getting the anvil too hot directly below the sample can lead to poor samples as can not allowing the arc sufficient time to completely melt the samples. In these cases, there were signs of microcrystalline structure. In some samples the center part of the foil showed fairly well defined spots superimposed on the diffuse halos indicating the presence of some crystallinity. This was found to be associated with hot spots on the anvil that contact the foil during quenching.

3.2 X-ray Diffraction

It is a fundamental principle that there is no long-range order in the structure of a glass. Knowing the positions of the atoms in one region of an amorphous solid is not helpful in predicting the positions in a distant region. However, some kind of order is to be expected at short range.

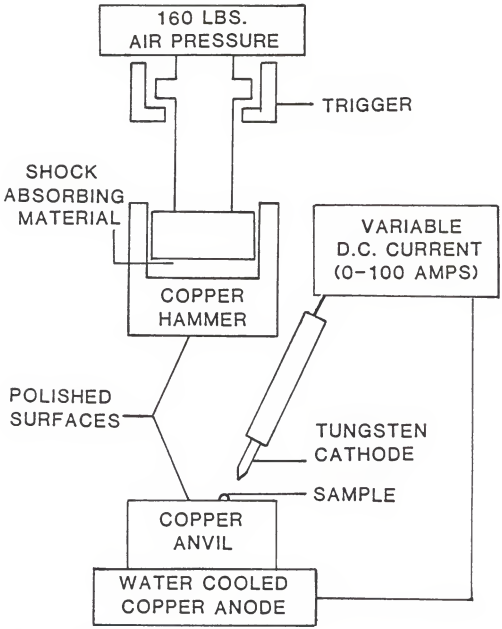

Fig. 3.1 Splat cooling apparatus.

A direct piece of information about the local short range order in amorphous solids has come from X-ray experiments. In a crystal, the diffractogram consists of a sequence of discrete sharp peaks resulting from the almost perfect correlation of the atomic positions throughout the volume of the crystal. In an amorphous solid the peaks are broad due to a distribution of interatomic distances and are located at slightly different positions.

To insure the alloy foils are amorphous, X-ray diffraction measurements were performed. Each sample discussed here was examined by X-ray diffraction using Cu-Kα radiation in conjunction with a proportional counter. In all cases the diffraction pattern showed only two broad diffuse peaks that fade into a featureless background, indicating a glassy structure. There were some resolvable peaks on the two major diffuse broad peaks in some of the measurements, but on repeating the measurements these small peaks did not occur at the same place. Therefore, we can safely conclude that these peaks were noise. The standard used was a Permaquartz sample that yielded a diffractogram with sharp peaks of high intensity. The intensity for the amorphous samples was at a much lower scale than that for the standard Permaquartz. Figure 3.2 shows the diffractograms of the amorphous $Gd_xCo_{35}Er_{65-x}$ alloys. The samples containing Er have shown peculiar ac susceptibility measurements (see section 4.5) comparable to the other rare-earths discussed. However, no structure was seen in the first peak or other resolvable peaks in addition to the two major diffuse peaks. Thus, we see no evidence for crystallinity or two amorphous phases in

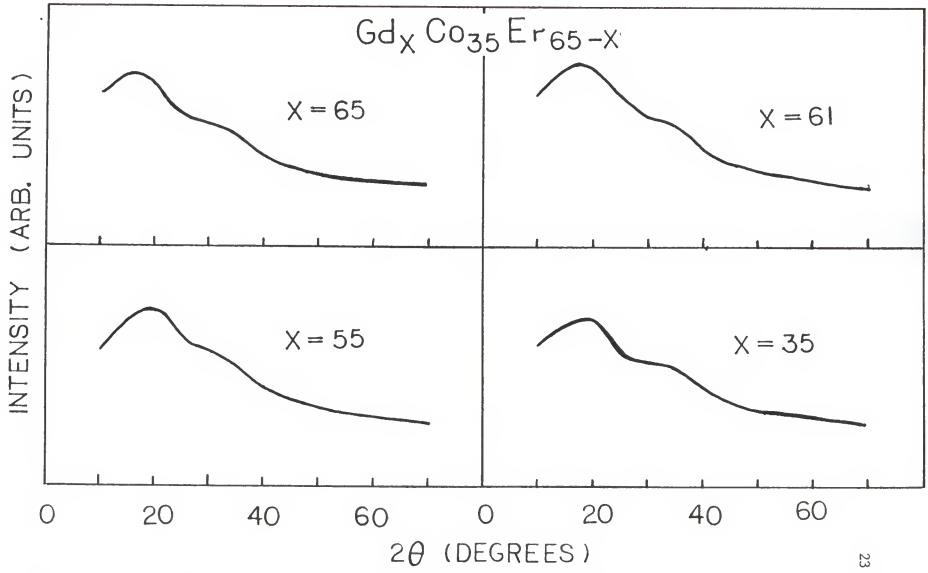

Fig. 3.2 X-ray diffractogram on amorphous $Gd_xCo_{35}Er_{65-x}$ with Cu-Kα radiation.

our X-ray studies of the Er system. Increasing the concentration of Er showed no noticeable effects on the amorphousness of the materials. It is noted that the peak position of the first diffuse peak shifted to slightly higher or lower values of diffraction angle showing slight differences in the amorphous structure of the samples. However, the instrument used was not capable of any detailed analysis.

3.3 Differential Scanning Calorimetry (DSC)

For any solid material there is always at least one crystalline phase that is more stable than the amorphous state. In other words, the crystalline form is favored thermodynamically (it is said to have a lower free energy).

For this thesis, Differential Scanning Calorimetry (DSC) measurements were done to further study the amorphous structure of the samples. The system is made up of a cell base module and a DSC cell. The cell base is an operating base for the DSC cell, connected by cable to the control console. It transmits heater voltages and thermocouple signals between the console and the cell. Output from the thermocouples is controlled and amplified by circuitry in the cell base. The DSC cell is used to measure differential heat flow. (See Figure 3.3.) In the cell, the sample and an empty reference pan sit on raised platforms on a constantan disc. Heat is transferred through the disc to the sample and reference. Differential heat flow is monitored by thermocouples located beneath the sample and reference pans.

When a substance changes phase, the transformation may be either endothermic (heat is absorbed) or exothermic (heat is given off). When

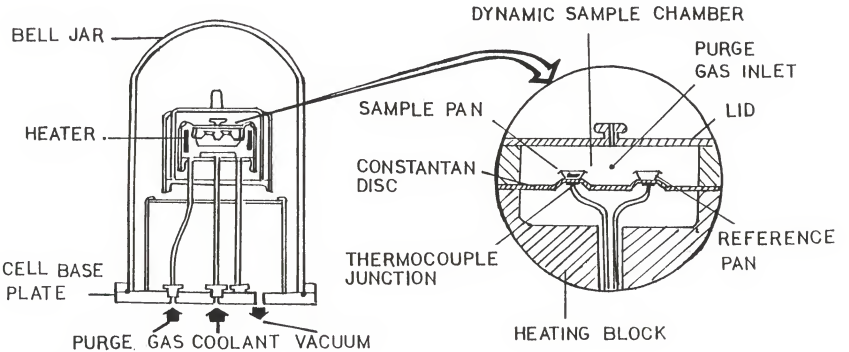

Fig. 3.3 Cross section, DSC cell.

an amorphous phase changes to a crystalline phase heat is given off as the atoms rearrange themselves in establishing a more stable configuration. From the DSC measurements (see Figure 3.4), we see an increase in heat flow at the glass temperature (T_g). (T_g was calculated from the construction shown in Figure 3.5.) This indicates that the metallic glasses have changed from an amorphous phase to a crystalline phase. We note that the glass temperatures vary from 220°C for Pr to 334°C for Er. This, we believe, to be directly due to the different atomic spacings. If we define the metallic radius as the half-distance between an atom and its neighbors, the metallic radius decrease almost linearly from 1.8279 Å for elemental Pr to 1.7566 Å for Er, with the exception of Ce which has a radius of 1.8247 Å. (See Table 3.1) [29]. Pr, which has the largest metallic radius compared with the rare-earths discussed here, has the lowest T_g and Er with the smallest metallic radius has the highest T_g. The slight difference in the heights of the peaks may indicate a small variation of amorphous structure. Occasionally we see a second smaller exothermic peak at higher temperature, but this is not seen in the Er_4 sample. (Er samples have shown quite unusual ac susceptibility measurements; section 4.5.) The endothermic peak present at higher temperatures indicates a decrease in heat flow and is a crystalline to crystalline phase change.

Increasing the concentration of different RE's also affects the T_g by the same principle. (See Figure 3.5.) Increasing the concentration of Er, which has a small metallic radius, increases T_g and the system becomes more stable. On the other hand, Pr, which has a larger metallic

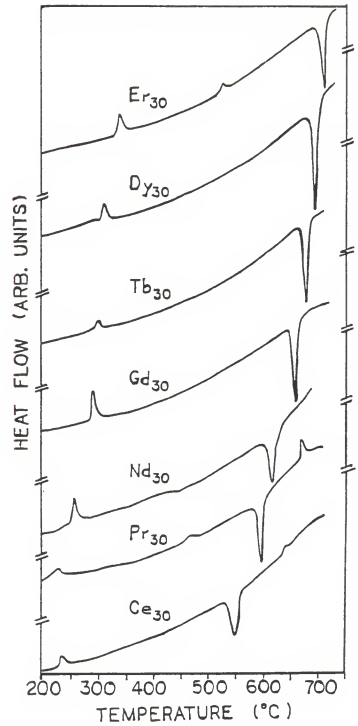

Fig. 3.4 DSC measurements on $Gd_{35}Co_{35}RE_{30}$ where RE = Ce, Dy, Er, Nd, Pr, Tb.

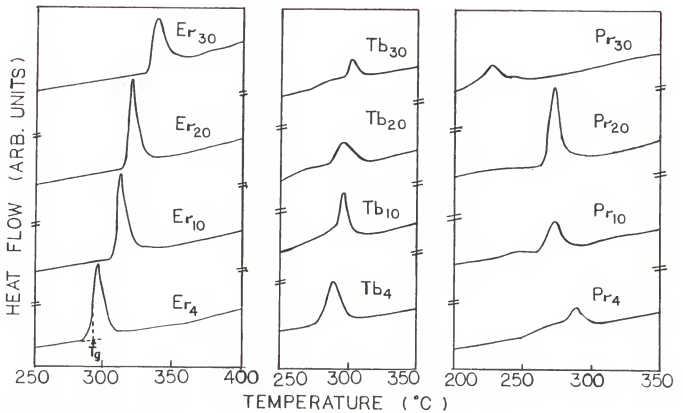

Fig. 3.5 DSC measurements on $Gd_xCo_{35}RE_{65-x}$ where Re = Er, Pr, Tb.

radius than Gd, becomes less stable with increase in concentration. Thus, we see a decreasing value of T_g with higher concentrations of Pr. Finally, Tb, which is close to Gd, shows very little change in T_g. The reason for the variation of T_g with metallic radius is not understood in detail and the glass forming ability of the rare-earths is a subject of considerable research.

Table 3.1 Metallic Radius for Ce, Dy, Er, Gd, Nd, Pr, Tb

Rare earth	Ce	Pr	Nd	Gd	Tb	Dy	Er
Metallic Radius (Å)	1.8247	1.8279	1.8214	1.8013	1.7833	1.7740	1.7566

3.4 AC Susceptibility

AC Susceptibility measurements were made on thin strips of these materials using an ac probe. The ac probe was designed to be lowered into a He storage dewar (see Figure 3.6) and the temperature is usually controlled by adjusting the height of the probe above the liquid He surface. The sample is placed inside the 'coil former' at the end of the probe. (See Figure 3.7.) The 'coil former' consists of two series opposition pick-up coils which are inside an outer driving coil (modulation coil). When no sample is present, the pick-up coils produce no outpout emf since the emf's generated are in opposition, so they cancel. With a magnetic sample within the bottom pick-up coil, the emf's become unbalanced and a signal is produced. χ_{ac} is then determined as

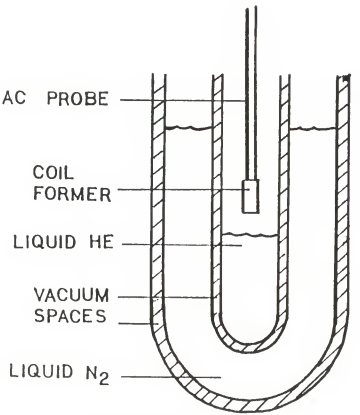

Fig. 3.6 Glass He dewar.

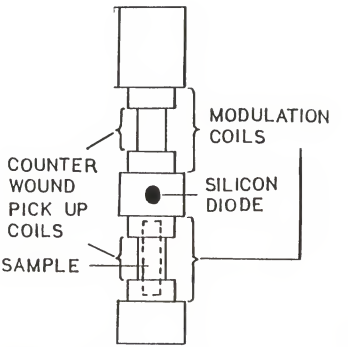

Fig. 3.7 Coil former for ac.

the difference between the two signals. The modulation coil was driven by the reference output of a lock in amplifier at low audio frequency around 280 Hz. The amplitude of this measuring field was $\sim$ 1 Oe.

The temperature was measured by a calibrated silicon diode with a 10 μA current which was placed close to the sample. While the probe was being moved up and down the voltages across the pick-up coils and the diode are continuously measured.

Rectangular strips about 1 mm by 12 mm were cut from the splat cooled foil and varnished (GE-7031 varnish) into a sample holder which is a plastic tube 2 mm in diameter and 13 mm long. The samples were placed with the long axis parallel to the applied ac magnetic field to minimize demagnetization. We use approximately 30 mg of material for this measurement.

One problem with rare-earth based metallic glasses is that they can be relatively fragile (as compared to transition metal based glasses) and this can lead to problems when preparing ac samples. Sometimes the varnish tends to detach from the sample during thermal cycling. Some of the Pr based glasses for instance were repeated several times before suitable data were obtained. This problem appeared in light rare-earth based glasses quite frequently (Ce, Nd, Pr) and is apparently related to a thin oxidation layer between the samples and varnish. Cracking of these samples during thermal cycling can also induce the varnish to be detached from the sample. The varnish could also be strained against the sample due to the different expansions of the sample holder and the sample. To ease this problem, the metallic strips were stacked together

in sandwich form before varnishing them in the sample holder. AC measurements provide an accurate method of determining the transition temperature (T_c) between different phases. Interestingly, taking the probe up or down too fast will give a T_c that deviates $\sim$ 10 K from the true T_c. Thus, all ac measurements were taken with the probe lowered and raised very slowly into or out of the liquid He dewar.

AC susceptibility measurements are important indicators of the ground state properties of magnetic systems. A transition to an infinite susceptibility phase, for instance, would show a large rise in the ac susceptibility to a constant value (the demagnetization limit) where it would remain as long as the susceptibility is infinite. The measured ac susceptibility χ_{ac} is given by

$$\chi_{ac} = \frac{dM}{dH_a} = \frac{dM}{d(H_i + NM)}$$

where the applied field $H_a = H_i + NM$, with N the geometrical demagnetization factor. The internal susceptibility $\chi_i = \frac{dM}{dH_i}$ is then given by

$$\chi_i = \frac{\chi_{ac}}{(1 - N\chi_{ac})}$$

Thus, we expect

(i) with χ_{ac} small, then $\chi_{ac} \ll N$, and $\chi_i \approx \chi_{ac}$

(ii) with χ_{ac} large, then $\chi_{ac} \approx \frac{1}{N}$, and $\chi_i \rightarrow \infty$

for the case of a transition into a ferromagnetic state at $T = T_c$ We define the transition temperature (T_c) to be the temperature of the peak value (χ_{ac}^{max}).

3.5 Vibrating Sample Magnetometer (VSM)

Magnetization measurements were carried out at 4.2 K with a vibrating sample magnetometer. In this method the sample (which may be taken to be a point dipole) is vibrated up and down between the centres of two counter wound pick-up coils in a constant magnetic field. Since the sample is always receeding from one coil and approaching the other, the emf's add. This induced emf is proportional to the moment on the sample. The magnetization is obtained via a lock-in amplifier. The sample used here is the same as that for ac susceptibility measurements. The sample within its holder was mounted vertically on a long vibrator rod so that the plane of the sample is aligned with the applied field to reduce demagnetization effects. The vibrator rod was deiven at 37 Hz.

CHAPTER 4

PHASE TRANSITIONS IN RANDOM ANISOTROPY MAGNETS

4.1 Experimental Results in the Small D/I Limit

AC susceptibility of amorphous $Gd_{65}Co_{35}$ is shown in Figure 4.1. This measured susceptibility shows a dramatic rise and sharp break near $T_c \sim 184$ K but only a mild decrease in χ_{ac}. This suggests a paramagnetic to ferromagnetic transition as T is lowered. χ_{ac} approaches the demagnetization limit (N^{-1}) which is indicated by the levelling of χ_{ac} below T_c. The true susceptibility, χ_i, therefore, is very large, possibly infinite. The relatively sharp transition taken together with the levelling of χ_{ac} below T_c suggest a ferromagnetic state at sufficiently low temperatures.

Figure 4.2 shows the temperature dependence of the inverse susceptibility for $Gd_{65}Co_{35}$ for temperatures above T_c. From this Curie-Weiss fit, $\theta \sim 189$ K.

The $Gd_{65}Co_{35}$ alloy appears to saturate with almost no increase in magnetization for applied fields greater than 30 kOe [17]. M saturates easily since $Gd_{65}Co_{35}$ is an S-state ion (small anisotropy). A hysteresis loop at 4.2 K is shown for $Gd_{65}Co_{35}$ in Figure 4.3. $Gd_{65}Co_{35}$ shows very little hysteresis with the measured coercive field H_c, being $\sim$ 200 Oe at 4.2 K. The near lack of hysteresis in $Gd_{65}Co_{35}$ is attributed to the absence of LRA in this alloy. The temperature dependence of remanence and coercivity of $Gd_{65}Co_{35}$ is illustrated in Figure 4.5. As temperature increases the magnetization decreases slowly and the coercive field increases slowly. It should be noted that none of

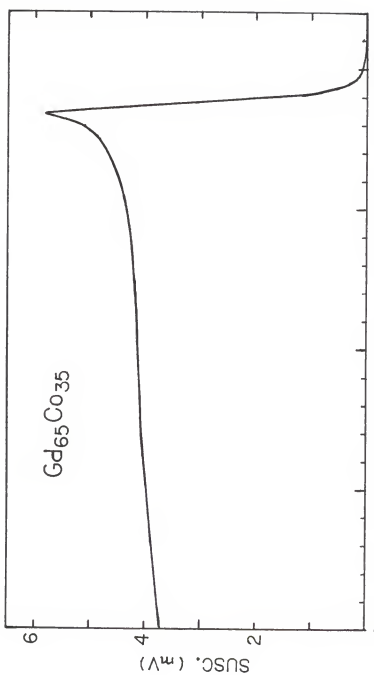

Fig. 4.1 AC susceptibility as a function of temperature for $Gd_{65}Co_{35}$.

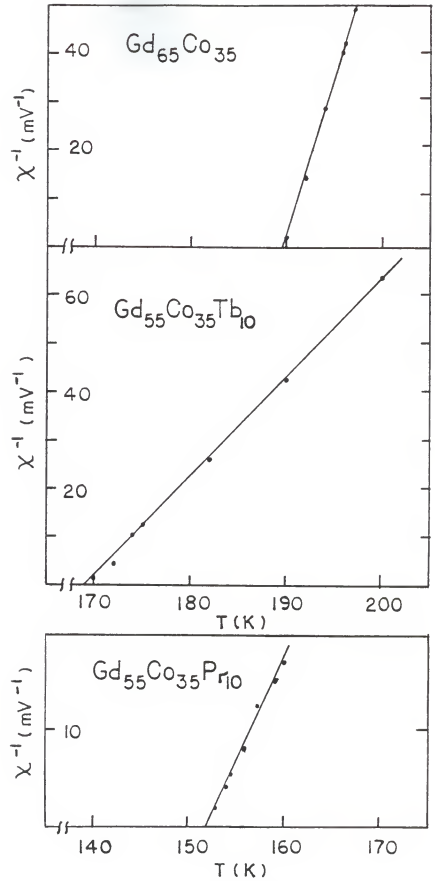

Fig. 4.2 Curie-Weiss fit for $Gd_{65}Co_{35}$, $Gd_{55}Co_{35}Tb_{10}$ and $Gd_{55}Co_{35}Pr_{10}$.

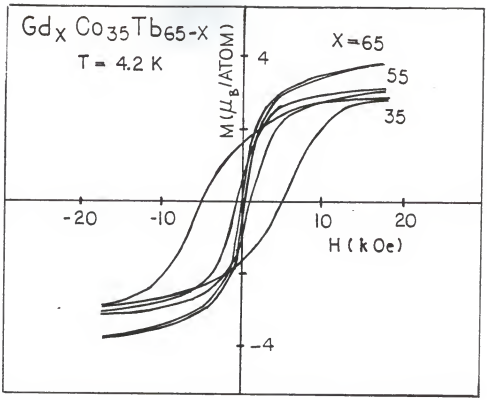

Fig. 4.3 Hystersis loops at 4.2 K for $Gd_xCo_{35}Tb_{65-x}$ where x = 65, 55, 35.

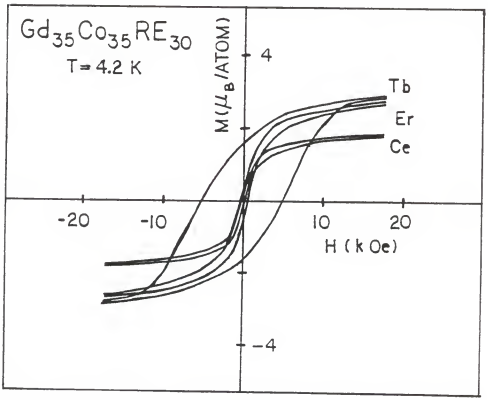

Fig. 4.4 Hystersis loops at 4.2 K for $Gd_{35}Co_{35}RE_{30}$ for RE = Tb, Er, Ce.

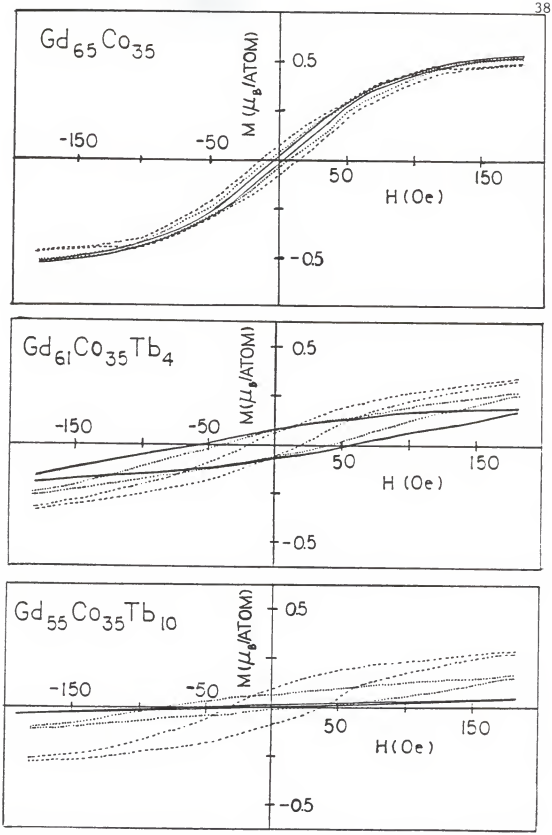

Fig. 4.5 Hystersis loops for (a) $Gd_{65}Co_{35}$, $Gd_{61}Co_{35}Tb_4$ and $Gd_{55}Co_{35}Tb_{10}$ at temperatures; 4.2 K ——; 32 K ·····, 100 K – – –.

these alloys are saturated in the fields shown in Figures 4.3 and 4.4. At higher fields in the alloys containing Tb it may be seen that the magnetization increases with temperature and this is characteristic of a frustrated system. (See 4.2.1.)

4.2 Experimental Results in the Large D/I Limit

The local random anisotropy (LRA) theory of Harris et al. [3] was developed assuming the presence at each magnetic site of a randomly directed uniaxial anisotropy which could compete with exchange forces to determine the direction of the local magnetic moment. In this section, the ratio of anisotropy strength to exchange, D/I is varied in our glasses by alloying, and the effect of this on the resulting magnetic states is discussed.

4.2.1 Tb Alloys ($Gd_xCo_{35}Tb_{65-x}$)

AC susceptibility measurements made on the Tb alloys are shown in Figure 4.6. The inset figure of Figure 4.6 sketches the theoretical result mentioned earlier of Dotsenko and Feigelman [10]. (See section 2.3.) The calculation breaks down near T_c, but there is some resemblance between the theory and our experimental results.

The alloys have a single peak which decreases as Tb is added. The fact that the peak heights lie well below the demagnetization limit suggest that they are not in an infinite susceptibility phase. Since the peak heights in the ac susceptibilitiess are reduced as more Tb is added, it is suggested that the ground state for more concentrated Tb alloys contains a larger concentration of randomly 'frozen' spin orientations. As the concentration of Tb increases, the magnetic ground states of these

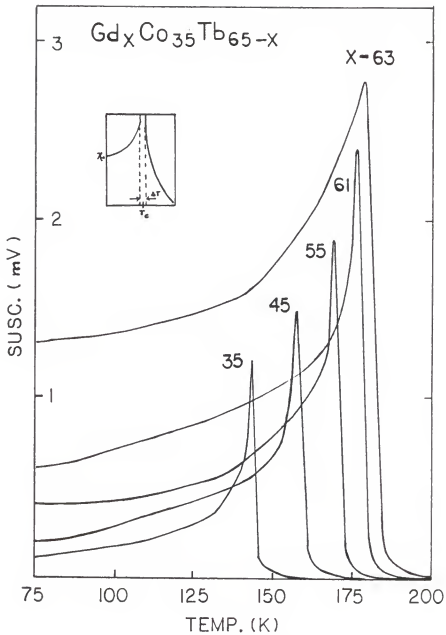

Fig. 4.6 AC susceptibility as a function of temperature for $Gd_xCo_{35}Tb_{65-x}$ where x = 63, 61, 55, 45, 35. The inset is an LRA calculation prediction of Dotsenko and Fiegelman (see text).

samples tend toward a speromagnetic state. The ordering temperature decreases correspondingly. The peaks become sharper with increasing Tb concentration. These are some of the sharpest peaks observed. Such transitions are much sharper than any of the canonical spin-glass transition (eg. Cu:Mn, Au:Fe) of which we are aware. The speromagnetic state is a frozen-in random spin structure much like a spin-glass state; the difference is that the latter is produced by the presence of an antiferromagnetic interaction.

For all RE-Co alloys the inverse susceptibility shows Curie-Weiss behavior for temperatures above T_c that is a linear dependence of χ^{-1} with temperature above T_c. Figure 4.2 shows representative examples of Curie-Weiss fits. At large D/I values the infinite susceptibility state is suppressed and there is a direct transition from the paramagnetic state to the speromagnetic state as is evidenced by the Tb glasses.

One feature which would allow us to discern the properties of the eventual spin-glass-like phase is the presence of hysteresis at temperatures below T_c. High field magnetization data at 4.2 K for $Gd_{65}Co_{35}$, $Gd_{55}Co_{35}Tb_{10}$ and $Gd_{35}Co_{35}Tb_{30}$ glasses are shown in Figure 4.3. The data display non-saturation at high fields of $\sim$ 17 kO_e and relatively large coercivities in the case of the Tb glasses. A number of theories of LRA [30] indicate that coercivity is proportional to the anisotropy strength D, the proportionality constant varies for different theories. The coercivities for $Gd_{55}Co_{35}Tb_{10}$ and $Gd_{55}Co_{35}Tb_{30}$ are 0.740 kOe and 5.04 kOe respectively. The coercivity for $Gd_{65}Co_{35}$ was $\sim$0.200 kOe in agreement with this system having a low D.

There is a slow linear rise in the measured moment of $Gd_{55}Co_{35}Tb_{10}$ and $Gd_{35}Co_{35}Tb_{30}$. This behavior is associated with the closing of the fan-like structure of anisotropically oriented spins in amorphous alloys which exhibit LRA [30]. Similar behavior has been seen in the rare-earth amorphous alloys such as $Zr_{40}Cu_{60-x}M_x$, where M = Tb or Gd, and in $DyCo_{3.4}$ [31]. Recent model calculations for the amorphous magnetic state have also emphasized the importance of LRA for these materials [22].

Measurements of magnetization of $Gd_{61}Co_{35}Tb_4$ and $Gd_{55}Co_{35}Tb_{10}$ at several temperatures are shown in Figure 4.5. These measurements show a more complex behavior with high temperature hysteresis loops being narrower with less coercivity than lower temperature loops. The decay of coercivity with temperature suggests a thermal activation of domains over energy barriers as suggested for $Tb_{75}Au_{25}$ [32] and (TbGa)Fe [33]. This behavior is more pronounced in the Tb_{10} sample than in the Tb_4 sample. It is not clear why the coercivity for $Gd_{65}Co_{35}$ shows a slight increase with temperature.

Thus, for Tb alloys (alloys containing non-S-state ions) there is a magnetic ordering (speromagnetic) at low temperatures and below the ordering temperature a large magnetic anisotropy develops leading to high coercivities.

4.2.2 Dy Alloys ($Gd_xCo_{35}Dy_{65-x}$)

Figure 4.7 shows χ_{ac} for the heavy rare-earth glass series $Gd_xCo_{35}Dy_{65-x}$ where x = 61, 55, 45 and 35. Similar to Tb glasses, the Dy glasses are not limited by the demagnetization factor but rather show a small peak indicating a transition to a speromagnetic state. Again,

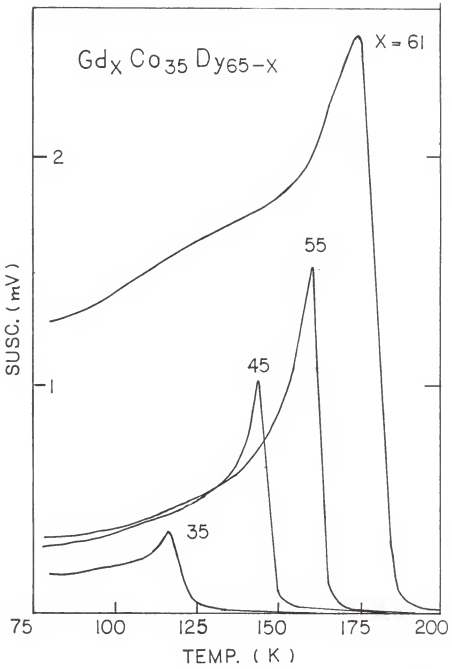

Fig. 4.7 AC susceptibility as a function of temperature for $Gd_xCo_{35}Dy_{65-x}$ where x = 61, 55, 45, 35.

speromagnetic phase refers to a frozen, random magnetic structure with no long-range order; this structure is similar to that of a spin-glass but we reserve the term for cases in which the origin of the spin scatter is LRA rather than frustration due to mixed interactions as in a spin-glass. The peak heights in χ_{ac} are reduced as more Dy is added. The reduction of the peak heights in Dy glasses is fastest when compared to the other glasses discussed in this chapter. Dy is exceptional because D is large and the moments then are strongly coupled to the local easy axis which are randomly oriented.

4.2.3 Nd Alloys ($Gd_xCo_{35}Nd_{65-x}$)

χ_{ac} for $Gd_xCo_{35}Nd_{65-x}$ (Figure 4.8) where x = 61, 55, 45 and 35 show a similar dramatic rise and sharp break near T_c with monotonically decreasing χ_{ac} below T_c. The susceptibility remains finite in all the Nd glasses and a small speromagnetic peak is present in each at sufficiently low temperatures. We have come to expect the peak heights to decrease as more anisotropy rare-earth is added, but we find a 'glitch' with the x = 55 sample. It is not fully understood why this is so. However, the T_c for the x = 55 sample falls accordingly with the others.

4.2.4 Pr Alloys ($Gd_xCo_{35}Pr_{65-x}$)

The measured susceptibility for Pr glasses is shown in Figure 4.9. A sharp transition is observed in all the Pr glasses and the peaks are not limited by the demagnetization factor. The low temperature susceptibility decreases suggesting the entrance into a speromagnetic

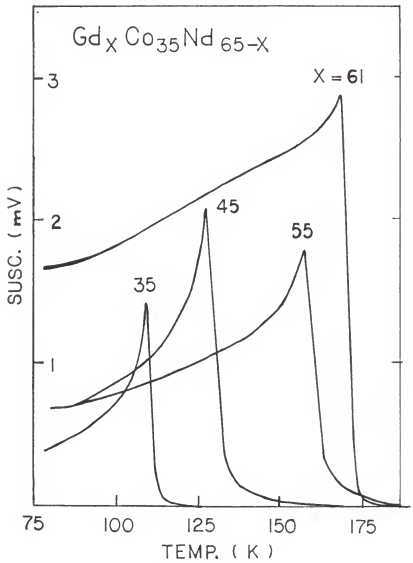

Fig. 4.8 AC susceptibility as a function of temperature for $Gd_xCo_{35}Nd_{65-x}$ where x = 61, 55, 45, 35.

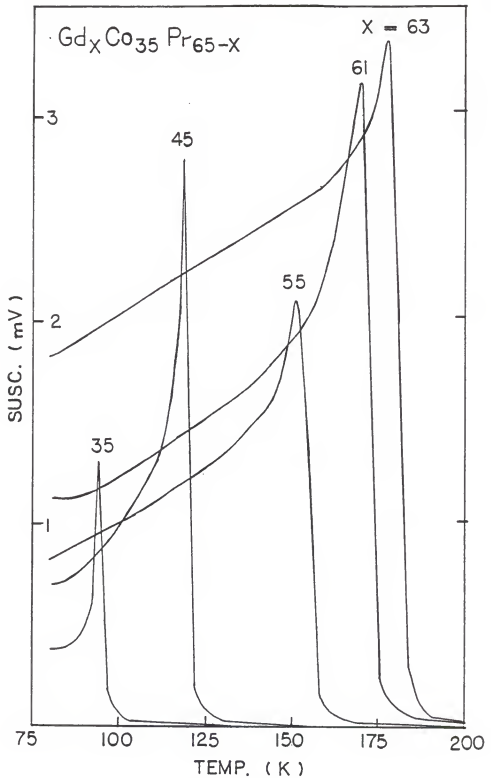

Fig. 4.9 AC susceptibility as a function of temperature for $Gd_xCo_{35}Pr_{65-x}$ where x = 63, 61, 55, 45, 35.

phase. The sharpness of the peaks seem to be enhanced as the Pr concentration is increased. The x = 45 sample shows an exceptional peak height comparable to others. It is not clear whether the x = 45 sample (Pr_{20}) or x = 55 sample (Pr_{10}) is the one to 'fall off' the trend of decreasing of peak height with more Pr concentration. Looking back on the DSC measurements on the Pr glasses (see Figure 3.5 of section 3.3), we see that Pr_{20} shows an exceptionally high exothermic peak compared to the other Pr glasses indicating the possibility of a different amorphous structure.

4.2.5 Ce Alloys ($Gd_xCo_{35}Ce_{65-x}$)

χ_{ac} for Ce glasses are shown in Figure 4.10. The the Ce glasses show a speromagnetic cusp with the susceptibility being less than the ferromagnetic demagnetization limit. The x = 45 sample shows a much slower approach to the transition. The peak height of Ce glasses decreases more slowly with more Ce concentration compared to other glasses we have discussed in this chapter. This suggests that Ce is less anisotropic than the other rare-earths studied. It should be noted that the Ce glasses may be more complicated than the other rare-earths studied since Ce may be quadrivalent.

The hysteresis loop at 4.2 K for $Gd_{35}Co_{35}Ce_{30}$ is shown in Figure 4.4. H_c for Ce_{30} is $\sim$ 0.37 kOe which is larger than the value for $Gd_{65}Co_{35}$ but much smaller than the Tb glasses at the same temperature. The magnetization of Ce_{30} shows no indication of reaching saturation even at a high field of $\sim$ 17 kOe.

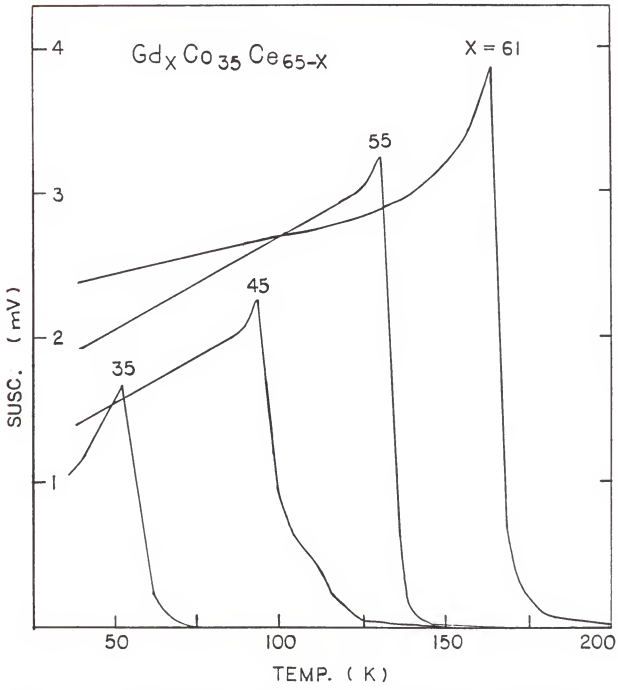

Fig. 4.10 AC susceptibility as a function of temperature for $Gd_xCo_{35}Ce_{65-x}$ where x = 61, 55, 45, 35.

4.3 Discussion of the Magnetic Phase Diagrams of $Gd_xCo_{35}RE_{65-x}$

The basic magnetic properties of rare-earth-rich RE-TM alloys are complicated by a large variety of spin orderings due to the random single-ion anisotropy inherent to RE ions, and can be interpreted as resembling the usual ferrimagnetic behavior only in the case of S-state ions like Gd.

The usual magnetic properties of the previously mentioned alloys containing non-S-state ions can be summarized as follows:

(i) Speromagnetic ordering appears at low temperatures, and

(ii) Below the ordering temperature a large magnetic anisotropy develops causing high coercivities and lack of saturation.

The HPZ model is able to explain many of the effects seen experimentally. In the small D/I (the ratio of anisotropy strength to exchange) limit we found a ferromagnetic phase at sufficiently low temperature (paramagnetic to ferromagnetic transition). For large D/I, the spins are pinned along their local axis at sufficiently low temperature and a frozen-in speromagnetic state (paramagnetic to speromagnetic transition) was present.

The critical temperature can indeed increase or decrease depending on the nature of structural disorder, composition, and the corresponding changes in the exchange interactions. T_c decreases as the strength of the exchange interaction decreases. Tb ion's which have the highest spin of 3 have the highest ordering temperature, and Ce with the lowest spin of 1/2 have the lowest ordering temperature. The ordering temperatures follow in a descending order for Tb, Dy, Nd, Pr and Ce corresponding to

the descending order of spins 3, 5/2, 3/2, 1 and 1/2 respectively. (See Figure 4.11.) This is expected for a system with an RKKY interaction which depend on S(S+1). If more RE is added the average exchange is further diminished and T_c will be lowered correspondingly. Similar results have also been achieved with amorphous $RE_{80}Au_{20}$ [34, 35, 36]. The ordering temperature T_c for each of the amorphous alloys we studied are summarized in Table 4.1 (Appendix A).

Legvold et. al [29] found that the magnetic ordering temperature varies nearly linearly with S(S + 1) versus magnetic ordering temperatures. Figure 4.12 is a plot of the weighted average of S(S + 1). The data seem to fall on a straight line, thus there is a resemblance between our experimental results and the theory.

4.4 Er Alloys ($Gd_xCo_{35}Er_{65-x}$)

Figure 4.13 shows results of ac susceptibility measurements on Er glasses of composition $Gd_xCo_{35}Er_{65-x}$ where x = 63, 61, 59, 55, 45 and 35. χ_{ac} for the samples x = 63, 61 and 59 (Er_2, Er_4 and Er_6 respectively) show peculiar behavior. In these samples we see what appears to be a double transition, that is paramagnetic to ferromagnetic-like to speromagnetic transitions. Figure 4.14 shows the magnetic phase diagram for the Er system. This magnetic character is quite different from that of the Er_{10}, Er_{20} and Er_{30} but the exact state is difficult to determine. DSC measurements (section 3.3) on the Er_4 sample show no second amorphous peak. There was no difference in the X-ray diffractograms of all the Er samples (section 3.2). With the above two measurements we see no evidence for a phase separation. Further

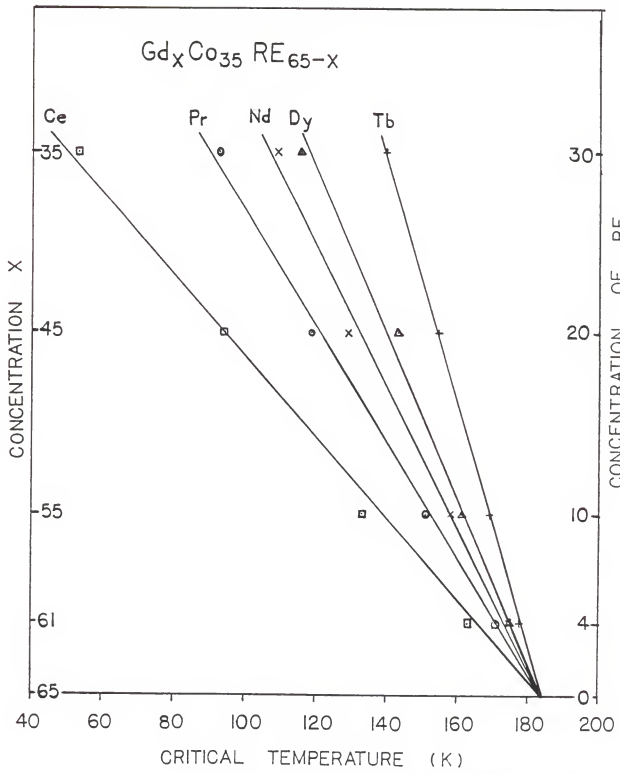

Fig. 4.11 Magnetic phase diagrams for $Gd_xCo_{35}RE_{65-x}$ where RE = Tb, Nd, Dy, Ce and Pr. (The solid lines are guides to the eye.)

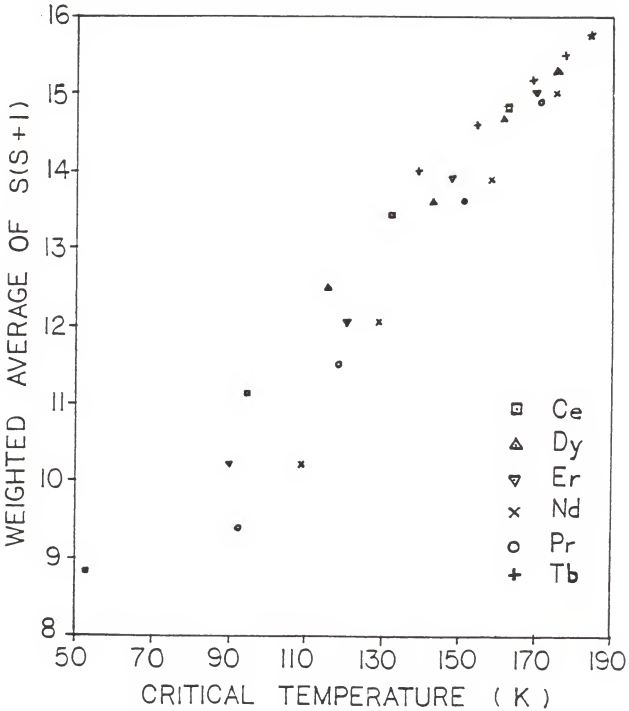

Fig. 4.12 The weighted average of S (S + 1) as a function of T_c for RE = Ce, Dy, Er, Nd, Pr, Tb.

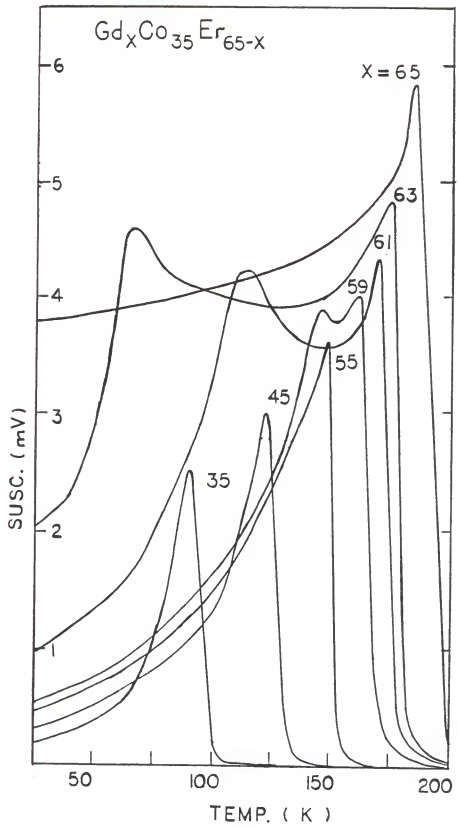

Fig. 4.13 AC susceptibility as a function of temperature for $Gd_xCo_{35}Er_{65-x}$ where x = 63, 61, 59, 55, 45, 35.

structural studies such as selected-area-electron diffraction and flourescence measurements would help in determining whether there are two magnetic phases present due to a phase separation. It is however possible to eliminate phase separations which produce crystalline precipitates since such crystalline regions would have well defined transition temperatures that do not vary with sample composition.

The strong reduction in χ_{max} observed in these glasses at sufficiently low temperatures indicate they are not ferromagnetic and suggest a speromagnetic ground state.

High-field magnetization data at 4.2 K for Er_{30} is shown in Figure 4.4. There is a considerable coercive field $\sim$ 0.59 kOe at 4.2 K but it is reduced from the corresponding Tb_{30} glass. The magnetization is still far from being saturated in a field of $\sim$ 17 kOe. Magnetic hardness in Er glasses is due to the anisotropy which tends to compete against exchange forces in an attempt to align spins along the local easy axis.

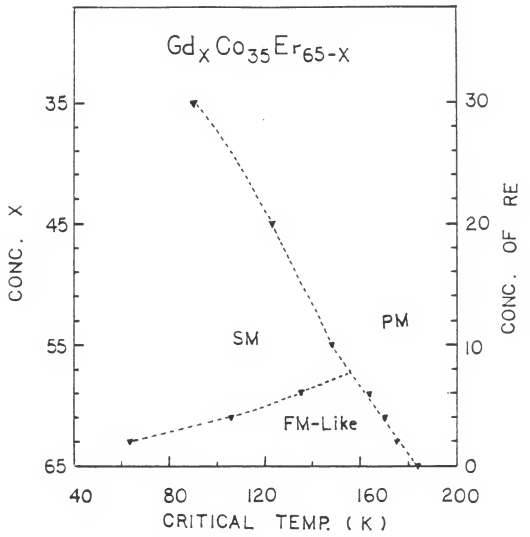

Fig. 4.14 Magnetic phase diagram for $Gd_xCo_{35}Er_{65-x}$ where x = 63, 61, 55, 45, 35.

CHAPTER 5

SCALING AT THE SPEROMAGNETIC TRANSITION

Because of the relative sharpness of the speromagnetic transitions seen in rare-earth-rich glasses (Chapter 4), we have studied the susceptibility behavior of representative Tb alloys in an applied dc field (H_{DC}). Since D/I is relatively large in these glasses, we take seriously the idea (mentioned earlier in section 2.5) that LRA glasses can be considered as equivalent in some sense, to Ising spin-glasses.

The ac susceptibility has been measured at 280 Hz in the temperature range $\sim$ 78 K - 200 K. The amplitude of the ac measuring field was $\sim$ 1 Oe. The dc field was varied in the range 0 - 100 Oe. The sensitivity for the signal amounted to 0.001 μV. No frequency dependence of the susceptibility maximum (peak height) is observed up to 280 Hz. Thus, we are seeing the limiting low frequency behavior of dM/dH at 280 Hz. Application of increasing dc field produces a slow 'rounding off' of the peak. It is interesting to note that for large values of H (50 Oe and 100 Oe), a shoulder began to develop in χ_s.

We show in Figures 5.1 - 5.3 the initial (H = 0) ac susceptibility versus temperature of Tb_{30}, Tb_{10} and Tb_4 respectively compared to several values of dc field applied parallel to the ac field. In order to study the field dependence of χ_s we use the definition (given in section 2.5)

$$\chi_s = \chi_{o(T)} - \chi(H,T) \qquad (7)$$

Here χ_o is the linear susceptibility for H = 0 and $\chi(H,T)$ the non-linear susceptibility. The non-linear χ does not diverge, whereas theory predicts that it does. A detailed physical interpreation of β

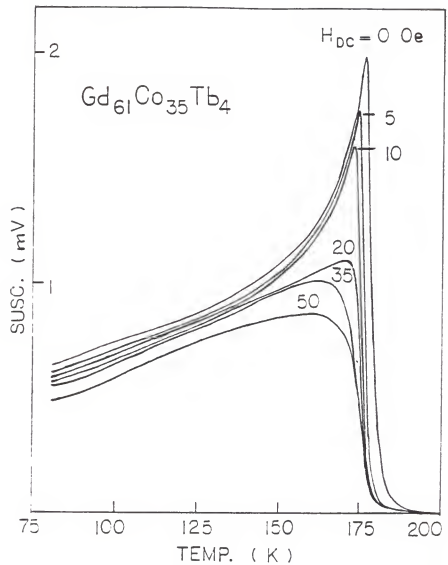

Fig. 5.1 Field-cooled ac susceptibility of $Gd_{61}Co_{35}Tb_4$ in various dc applied fields.

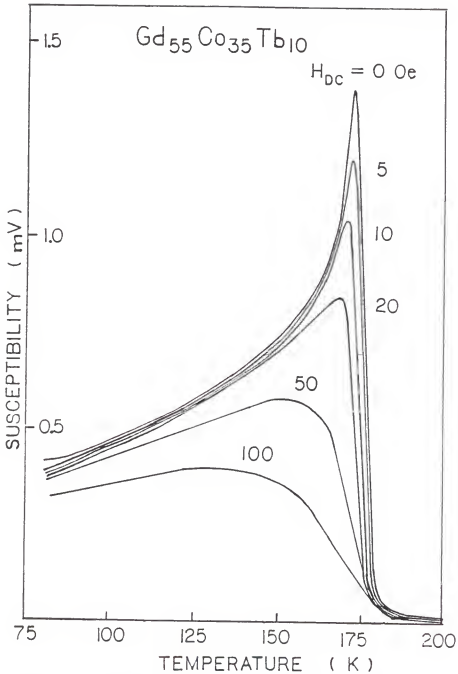

Fig. 5.2 **Field-cooled ac** susceptibility of $Gd_{55}Co_{35}Tb_{10}$ in various dc applied fields.

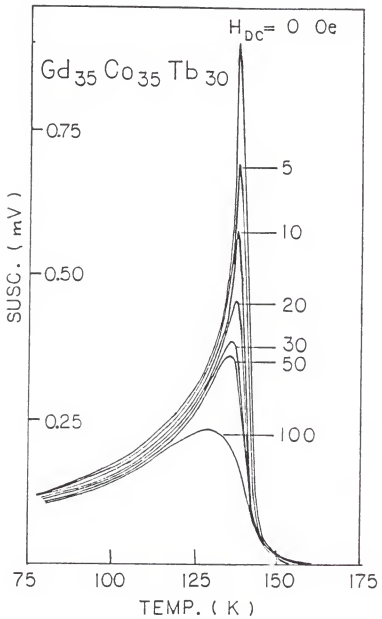

Fig. 5.3 Field-cooled ac susceptibility of $Gd_{35}Co_{35}Tb_{30}$ in various dc applied fields.

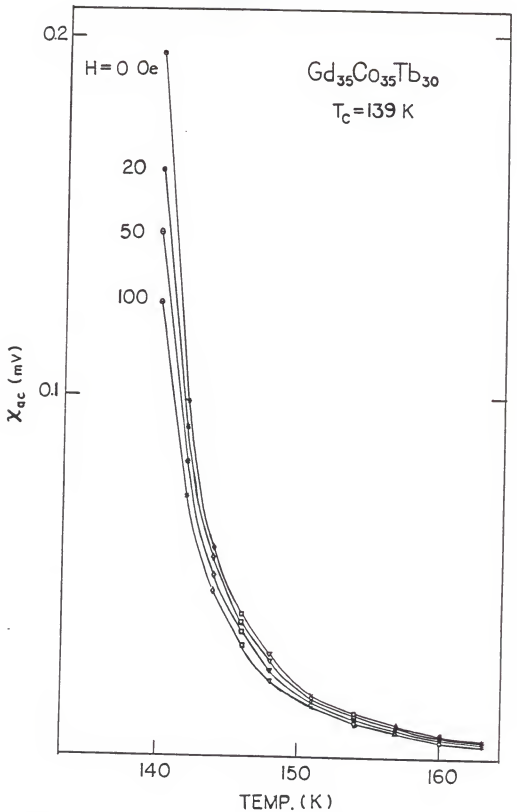

Fig. 5.4 AC susceptibility versus temperature for $Gd_{35}Co_{35}Tb_{30}$ for several values of H.

and δ is not possible due to this problem. Consequently, previous workers who have worked on Cu-Mn systems have not made scaling analyses close to T_c but have usually studied data in the range 1.1 - 1.4 T_c. For the moment then we shall consider the β and δ values as additional parameters in describing the magnetization in these and our systems. Earlier on we have measured ac susceptibility in the range of 78 K - 300 K with varying dc fields to observe how susceptibility depends on the changing fields. Since we want $\chi_o(T) - \chi(H,T)$ it makes sense to fix T and measure $\chi(H,T)$ at a series of H values and then change to the next T. For scaling purposes the isothermal field variation of the ac susceptibility has been measured for 6 - 10 approximately 'equally spaced' values of temperature 1.01 - 1.20 T_c as shown in Figure 5.4.

In Figures 5.5 - 5.7 we have represented the data $\chi_s / \epsilon^{\beta}$ versus $H/\epsilon^{(\beta\delta/2)}$ on a log-log scale. The data show an approximate collapse onto a single line. One can see a gradual improvement in the quality of scaling as more Tb is added to the system. So as the ac susceptibility becomes much smaller than the demagnetization limit the scaling improves. As may be seen from Table 5.1 our values of β and δ are close to those found in Cu-Mn systems where exchange fluctuations are important.

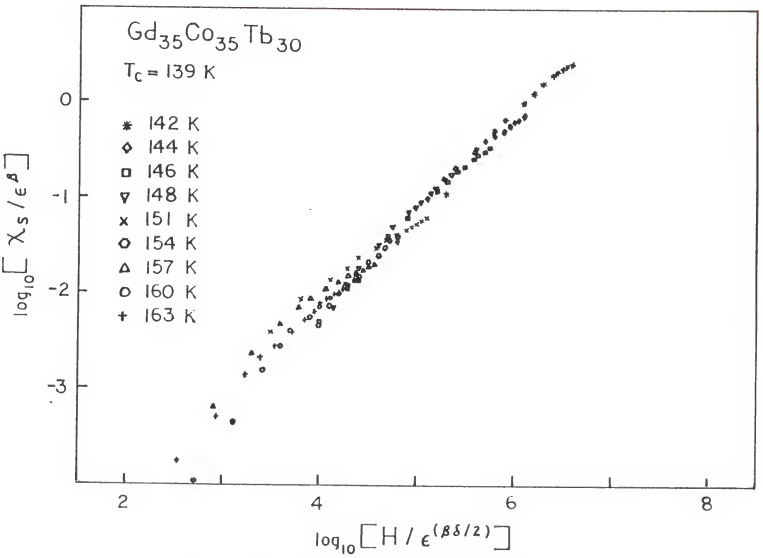

Fig. 5.5 Scaling function χ_s/ϵ^{β} versus $H/\epsilon^{(\beta\delta/2)}$ on log-log scales for $Gd_{35}Co_{35}Tb_{30}$ with β = 1.3 and δ = 4.7.

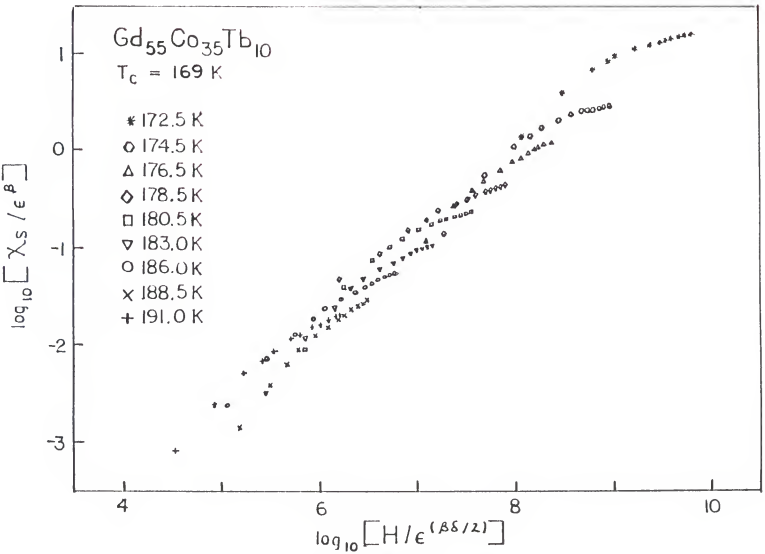

Fig. 5.6 Scaling function χ_s/ϵ^{β} versus $H/\epsilon^{(\beta\delta/2)}$ on log-log scales for $Gd_{55}Co_{35}Tb_{10}$ with $\beta = 1.5$ and $\delta = 6.5$.

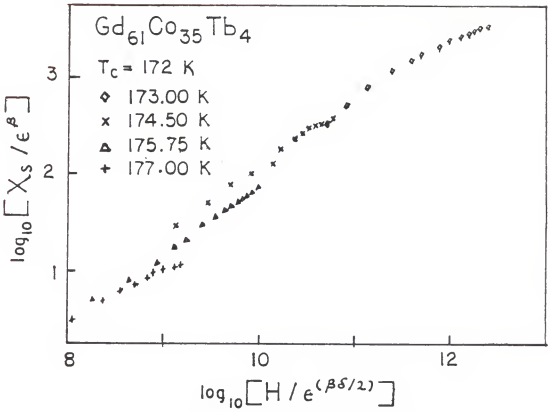

Fig. 5.7 Scaling function χ_s/ϵ^{β} versus $H/\epsilon^{(\beta\delta/2)}$ on log-log scales for $Gd_{61}Co_{35}Tb_4$ with β = 1.5 and δ = 6.5.

	Our Work			Barbara et al.	Berton Odin et al.	Omari et al.
Reference				37	38	39
System	$Gd_{61}Co_{35}Tb_4$	$Gd_{55}Co_{35}Tb_{10}$	$Gd_{35}Co_{35}Tb_{30}$	Cu Mn 4.6%	Cu Mn 0.25%	Cu Mn 1%
$\frac{H}{T_c}$ Oe/K	0.01–0.58	0.01–0.59	0.01–0.72	4–400	70–1500	20–7000
$\frac{T}{T_c}$	1.005–1.020	1.02–1.13	1.02–1.17	1.03–2.00	1.04–2.00	1.10–4.00
β	1.5 ± 0.1	1.5 ± 0.1	1.3 ± 0.1	1.1 ± 0.2	1	0.5–1
δ	6.5 ± 0.5	6.5 ± 0.5	4.7 ± 0.2	4.15 ± 0.15	4.65 ± 0.35	5.7 ± 0.5

Table 5.1 The values of β and δ of $Gd_xCo_{35}Tb_{65-x}$ where x = 61, 55, 35 as determined experimentally are compared to the β and δ values obtained by others. In lines 3 and 4, we specify the actual range of H/T_c and T/T_c values utilized in this determination.

CHAPTER 6

CONCLUSION

We have developed a number of amorphous rare-earth systems where the D/I ratio may be varied. The systems are $Gd_xCo_{35}RE_{65-x}$ where RE = Ce, Pr, Nd, Tb, Dy and Er. These systems were chosen for study since all the rare-earths (except Ce) are trivalent so that electronic structure changes are minimized on alloying. Amorphous structure variations are probably small on alloying and are systematic as seen in the DSC. For all RE-Co alloys, the inverse susceptibility shows Curie-Weiss behavior for temperatures above T_c. The experimental results are in agreement with the predictions of the LRA model [3]. In the small D/I limit ($Gd_{65}Co_{35}$) we have ferromagnetic behavior with large, possibly infinite susceptibility at sufficiently low temperature. In the large D/I limit the infinite susceptibility state is suppressed and there is a direct transition to a speromagnetic state as is evidenced by the Tb, Pr, Ce, Dy and Nd glasses. The Er alloy showed double transition behavior which is not understood at the present time. The height of the ac susceptibility decreases with increasing D/I (more anisotropic rare-earth added) in accordance with the theory of Aharony and Pytte but we have not attempted to qualitatively check the prediction $\chi \sim (I/D)^4$. Ce with the smallest D/I value has the highest susceptibility peak whereas Dy with the highest D/I value has the lowest susceptibility peak. We have shown that T_c is proportional to the weighted average of $S(S + 1)$ as expected for an RKKY interaction.

One can also see the effects of D/I in hysteresis with the Ce and Er systems showing a small hysteresis consistent with a small D/I and the Tb system showing a large hysteresis and relatively small susceptibility consistent with a large D/I. The ability to control the composition suggests that we are on our way to exploitation of rare-earth glasses.

A scaling analysis on the non-linear magnetization above T_c was done for the Tb systems. β and δ values were obtained which are close to those found in spin-glass systems. It was found that the quality of the scaling analysis apparently improved for systems containing more Tb. This may be related to the fact that the system is approximating more closely to an Ising-like system as the anisotropy becomes stronger. In support of this it has been noted that the mean field theories of Ising systems with exchange fluctuations and LRA systems are equivalent in the limit of large anisotropy as discussed in section 2.4.

APPENDIX A

Table 4.1 Transition Temperatures for $Gd_xCo_{35}RE_{65-x}$

RE	Ce	Pr	Nd	Tb	Dy	Er (T_1)	Er (T_2)
X							
65	184.0						
63		179.0		178.5		175.5	63.0
61	163.0	171.0	175.0	176.0	175.0	170.0	116.0
59						163.5	135.0
55	132.0	151.0	158.0	169.0	161.0	148.0	
45	94.5	118.5	129.0	154.5	143.0	123.0	
35	53.0	92.5	109.0	139.5	115.5	90.0	

REFERENCES

[1] A.I. Gubanov, Fiz Tver. Tela 2, 502 (1960).

[2] J.J. Rhyne, S.I. Pickart and N.A. Alperin, Phys. Rev. Lett., 29, 1562 (1972).

[3] R. Harris, M. Plischke and M.J. Zuckermann, Phys. Rev. Lett., 31, 160 (1973).

[4] D.J. Sellmyer and S. Nafis, J. Appl. Phys., 57(1), April 1985.

[5] E.M. Chudnovsky and R.A. Serota, J. Phys., C16, 4181 (1983).

[6] Y. Imry and S.K. Ma, Phys. Rev. Lett., 35, 1399 (1975).

[7] E. Pytte, in T. Riste (ed.), Ordering in Strongly Fluctuating Condensed Matter Systems, Plenum, New York, 1979, p. 445.

[8] A. Aharony and E. Pytte, Phys. Rev. Lett., 45, 1583 (1980).

[9] A. Aharony and E. Pytte, Phys. Rev., B27, 5872 (1983).

[10] V.S. Dotsenko and M.V. Feigelman, J. Phys., C16, L803 (1983).

[11] M.A. Ruderman and C. Kittle, Phys. Rev., 96 (1954) 95.
T. Kasuya, Prog. Theor Phys., 16 (1956) 45.
K. Yosida, Phys. Rev., 106 (1957) 893.

[12] R.A. Pelcovits, E. Pytte, J. Rudnick, Phys. Rev. Lett., 40, 476 (1978); 48, 1297 (1982).

[13] R. Rammel and J. Souletie in Magnetism of Metals and Alloys, Ed. M. Cryot, p. 475, North-Holland (1982).

[14] J.H. Chen and T.C. Lubensky, Phys. Rev., B16, 2106 (1977).

[15] A. Aharony, Phys. Rev. B(12), 1038 (1975).

[16] M.J. O'Shea and D.J. Sellmyer, J. Appl. Phys., 57(1) April 1985.

[17] J.A. Gerber, D.J. Miller and D.J. Sellmyer, J. Appl. Phy, 49(3), (1699-1701), March 1978.

[18] J. Chalupa, Sol. State Comm., Vol. 24, pp. 429-431, 1977.

[19] G. Hadjipanayis, S.G. Cornelison, J.A. Gerber and D.J. Sellmyer, Journal of Magnetism and Magnetic Materials, 21 (101-107), 1980.

[20] B.G. Wybourne, Phys. Rev., 148 (1966) 317.

[21] J.A. Gerber, S.G. Cornelison, W.L. Burmester and D.J. Sellmyer, J. Appl. Phys., 50(3), (1608-1610), March 1979.

[22] R. Hasegawa, B.E. ARgyle and L.J. Tao, AIP Cont. Proc. 24, 110-112 (1974).

[23] C.M. Hurd, Contemp. Phys., 482-483, 1982, Vol. 23, No. 5.

[24] A.K, Bhattacharjee, R. Jullien and M.J. Zuckermann, J. Phys. F. Metal Phys., 7, 393-399 (1977).

[25] M.J. O'Shea, S.G. Cornelison, Z.D. Chen and D.J. Sellmyer, Sol. State. Comm., 46 (1983) 313.

[26] D.J. Sellmyer and M.J. O'Shea, J. Less Common Metals, 94 (1983) 59.

[27] K.H.J. Buschow, J. Appl. Phys., 51(5), (2795-2798), May 1980.

[28] M. Ohring and A. Haldipur, Rev. Sci. Instr. 42, 530 (1971).

[29] S. Legvold, Ferromagnetic Materials, Vol. 1, (E.P. Wohlfarth), North-Holland (1980).

[30] E. Callen, Y.J. Kiu and J.R. Cullen, Phys. Rev., B16, 263-270 (1977).

[31] G.R. Gruzalski, J.D. Patterson and D.J. Sellmyer; J.M.D. Coey, J. Chappert, J.P. Rebouillant and T.S. Wang, Phys. Rev., Lett., 36, 1061-1064 (1976).

[32] D.J. Sellmyer, G. Hadjipanayis and S.G. Cornelison, J. Non-crystalline solids, 40, 437 (1980).

[33] S.G. Cornelison, D.J. Sellmyer and G. Hadjipanayis, J. Appl. Phys. 52(3), 1823 (1981).

[34] S.J. Poon and J. Durand, Phys. Rev., B18 (1978) 6253.

[35] J.M. Friedt, M. Maurer, J.P. Sanchez, A. Berrada, A. Qachao, P. Panisod and J. Durand. J. Physique, 41 (1980) C8-638, J.M. Friedt, M. Maurer, J.P. Sanchez and J. Durand, J. Phys., F12 (1982) 821.

[36] A. Berrada, J. Durand, N. Hassanain and B. Leogel, J. Appl. Sphys. 50 (1979) 7621; Rare Earths in Mod. Sci. and Tech., Vol. 2, Plenum, New York 1979.

[37] B. Barbara, A.P. Malozemoff, Y. Imry, Phys. Rev. Lett. 47 (1981) 185, J. Appl. Phys. 53 (1982) 7672.

[38] A. Berton, J. Chaussy, J. Odin, R. Rammal and R.J. Tournier, Physique Lett. 43 (1982) L-153.

[39] R. Omari, J.J. Prejean and J. Souletie, Journal De Physique I, 44, No. 9, SEP 1983.

RANDOM MAGNETIC ANISOTROPY EFFECTS IN GLASSES BASED ON $Gd_{65}Co_{35}$

by

FAUZIAH OTHMAN

B.S., Kansas State University, 1983

AN ABSTRACT OF A MASTER'S THESIS

submitted in partial fulfillment of the

requirements for the degree

MASTER OF SCIENCE

Department of Physics

KANSAS STATE UNIVERSITY
Manhattan, Kansas

1985

Results of ac susceptibility and magnetization measurements are presented on the amorphous $Gd_xCo_{35}RE_{65-x}$ splat-cooled alloys where RE represents the anisotropic rare-earth Ce, Pr, Nd, Tb, Dy, Er and $65 \geq x \geq 35$. With decreasing x magnetic anisotropy is introduced into $Gd_{65}Co_{35}$ in a controlled fashion. X-rays show the sample to be amorphous. In all of the systems studied except Er the effect of the rare-earth was to transform the single ferromagnetic transition of $Gd_{65}Co_{35}$ to a spin-glass-like or speromagnetic transition. We have studied the non-linear susceptibility above the ordering temperature and a scaling analysis yields an approximate collapse of the isotherms with beta and delta values of 1.3 - 1.5 and 4.7 - 6.5 respectively in the Tb systems with x = 35, 55, 61. These values are close to those of dilute crystalline Cu-Mn alloys. The Er systems shows qualitatively different behavior with two transitions occurring for $x \geq 57$ and a single transition for $x < 57$. These results including possible explanations for the double transition behavior in the Er system are discussed.